C. R. Mecanique 347 (2019) 49–61

Contents lists available at ScienceDirect

Comptes Rendus Mecanique

www.sciencedirect.com

Simulating the dynamic behavior of planetary gearbox based on improved Hanning function

Oussama Graja [a,*], Bacem Zghal [a], Kajetan Dziedziech [b], Fakher Chaari [a], Adam Jablonski [b], Tomasz Barszcz [b], Mohamed Haddar [a]

[a] National School of Engineers of Sfax, Laboratory of Mechanics Modelling and Production, Sfax, Tunisia
[b] AGH University of Science and Technology, Krakow, Poland

ARTICLE INFO

Article history:
Received 22 May 2018
Accepted 29 September 2018
Available online 2 November 2018

Keywords:
Planetary gearbox
Vibration signals
Amplitude modulation
Side-bands
Dynamic response
Dynamic model

ABSTRACT

Planetary gearboxes are widely used in industrial machines. They usually work in harsh environments giving rise to damages and high maintenance costs. Condition monitoring is a key action allowing one to detect the presence of such damage ensuring healthy running conditions. The knowledge of the dynamic behavior of such a gearbox can be achieved using modeling tools as a primary step before conditioning the monitoring subject. In addition, modeling a gear set can help in the stage of design in order to optimize physical and geometric parameters of the system. Therefore, in this work, a two-dimensional lumped parameter model is adopted to build all vibration sources. The time-varying mesh stiffness is approximated as a square wave form. A novel mathematical formulation is proposed to model the amplitude modulation phenomenon due to the rotational motion of the planets around the center of the gearbox. Finally, the overall vibration signal is concluded as a summation of all vibration components influenced by the modulation function.

1. Introduction

Research and development in the field of planetary gear transmissions is continuously growing up. This interest is justified by the place taken by this kind of transmission in many industrial fields due to its important reduction ratio and compactness. This kind of gearbox differs from the parallel one by its more complex kinematic operation, i.e. one planet has not only a rotational motion with respect to its center, but also it revolves around the center of the gearbox. In addition, the multiple mesh between sun and planets with similar vibration forms, as well as the multiple ring-planet meshes, makes its dynamic behavior complex, failure prediction and failure detection a hard task.

Several researches were dedicated to the understanding of this dynamic behavior using a lumped parameter model-based approach. The dynamic models proposed in the literature can be divided into two groups according to the tooth geometry. For spur gears, a two-dimensional lumped parameter model is considered. Components are joined using stiffness and damping functions put in parallel as in [1], [2], [3], [24] and [32], or using only stiffness and adding damping as a Rayleigh proportional one [4], [6], [9], [12], [13], [20]. When the investigated gears are helical, two-dimensional models can not be

* Corresponding author.
E-mail address: grajaoussama@gmail.com (O. Graja).

https://doi.org/10.1016/j.crme.2018.09.006

sufficient to describe the real dynamic behavior of the planetary gearbox, since the mesh force is, in this case (helical gear), not parallel to the plane of rotation. Hence, researchers used a three-dimensional lumped parameter model as in [10], [11], and [30].

Liang et al. [1] developed the same lumped parameter model as that used by Lin and Parker [24] with some distinctions in order to simulate the vibration signal in both healthy and damaged cases. In a later work, Liu et al. [2] developed a non-linear lumped parameter model to build all vibration sources. They modeled the vibration transmission path effect as a combination of two components: one inside the gearbox and the other one through the casing. In order to highlight the modulation effects, they build the vibration signal as the summation of vibration from each component influenced by its transmission path. Viadero et al. [31] developed a multi-body model taking into account some offshore considerations in order to investigate the non-stationary dynamic behavior of a wind turbine power drivetrain. The dynamic behavior of the gearbox was simulated, including some transient regimes such as start-up and emergency stop. To investigate the effects of tooth profile deviations and support flexibility in [32] and the effect of run out and index errors [33], Fernandez et al. used a non-linear dynamic model. Zhang et al. [4] proposed a dynamic model of two-stage planetary gear to investigate the dynamic response in order to avoid resonance. Then, they compared their analytical model with a finite element simulation. Hence, they classified types of mode shapes into five groups and they concluded that the number of planets has an effect on natural frequencies. Since planets have a rotational motion around the center of the gear train, a transducer placed on the fixed ring collects a vibration signal modulated by the carrier frequency. To describe the mechanisms leading to this phenomenon, Inalpolat and Kahraman [5] proposed a simplified mathematical model that includes physical parameters such as planet position angles, number of planets, and number of teeth of each gear. Thus, they classified gear sets into five groups depending on their side-band activity in terms of spectral amplitude and frequencies. Later, Inalpolat and Kahraman [6] developed a non-linear dynamic model to predict sidebands around mesh frequency and harmonics of a planetary gear set having some manufacturing errors. Different gear manufacturing errors were introduced numerically. Since the gear error has a specific frequency, it contributes to the amplitude and frequency modulation. The sideband activity was also investigated by Feng and Zuo [7]. They modeled vibration signal taking into account amplitude and frequency modulation due to both damage and vibration transmission path effect, since the latter is time varying. Thereafter, they validated their numerical results using both machinery and test rig experimental signals. In a later work, Pattabiraman et al. [8] scrutinized the side band activity. Considering that a vibration caused by a meshing phenomenon is able to hide gear defect signals, they developed a new technique of signal processing named Side-band Energy Ratio (SER) allowing one to intensify frequency components of faults in a spectrum. According to Lin and Parker [24], the variation of the mesh stiffness is the most important source of vibrations in gear systems. In order to evaluate the mesh stiffness, the analytical model (AM) and the finite element method (FEM) have been adopted by researchers. Meagher et al. [25] used FEM to build a dynamic model to define the mesh stiffness variation. Jia and Howard [26] adopted a 3D-finite element model to evaluate the mesh stiffness function in the case of damaged gears. Zhan et al. [27] developed a technique to evaluate exactly the time-varying mesh stiffness based on NX, ANSYS, and quasi-static algorithm. Parker et al. [28] applied the FEM to compute the mesh stiffness in order to evaluate the dynamic response of a spur gear pair. Although, FEM provides good results, but it presents some disadvantages like CPU time consumption. AM was shown to be simpler compared to FEM, while providing good results [14], [15], [16], [17] and [18]. Chaari et al. [19] developed an AM model to compute the degradation of the mesh stiffness due to spalling and breakage. Later, Chaari et al. [22] evaluated mesh stiffness reduction due to cracked tooth by deriving an analytical formulation of the gear mesh stiffness. Works of Chaari et al. in [19] and [22] were focused only on external–external meshes. Since gears can be spur or helical, and also since the contact can be external or internal, Marques et al. [29] developed an analytical model to evaluate the mesh stiffness function of each case mentioned previously. In the work of Abousleiman et al. [34], authors proposed a hybrid 3D finite elements and lumped parameter model in order to analyze both the quasi-static and dynamic behaviors of both epicyclic and planetary gear-sets. They presented a new methodology to compute mesh stiffness as the mating flank position is time varying. The ring gear sub-structure modeled by FEM is connected to planets that are considered by a lumped parameter model. Cooley et al. [35] compared two calculation approaches of the mesh stiffness: average and local slope for respectively static and dynamic analysis. Both approaches lead to different vibration models. Hence, they proposed a hybrid formulation combining finite elements and contact mechanics approach to compute the time-varying mesh stiffness. In another work, Ayoub et al. [30] investigated the effect of mesh stiffness on natural frequencies under different loading conditions.

This work is organized as follows. In section 2, a lumped parameter dynamic model of a single-stage planetary gear is presented in order to simulate its dynamic behavior without taking into account the transmission-path effect. The time-varying mesh stiffness in this model is approximated as a square wave form. In section 3, a novel mathematical formulation of the modulation phenomenon is derived from the dimensional parameters of the planetary gearbox; this is the main purpose of this paper. The influence of the modification of some geometric parameters of the planetary gear-set on the modulation function is investigated. In section 4, the overall vibration signal is constructed, taking into account the modulation effect induced by the rotational motion of the planet around the center of the planetary gearbox. Finally, the resultant vibration signal is analyzed; its characteristics are revealed and compared with the experimental results presented in [23].

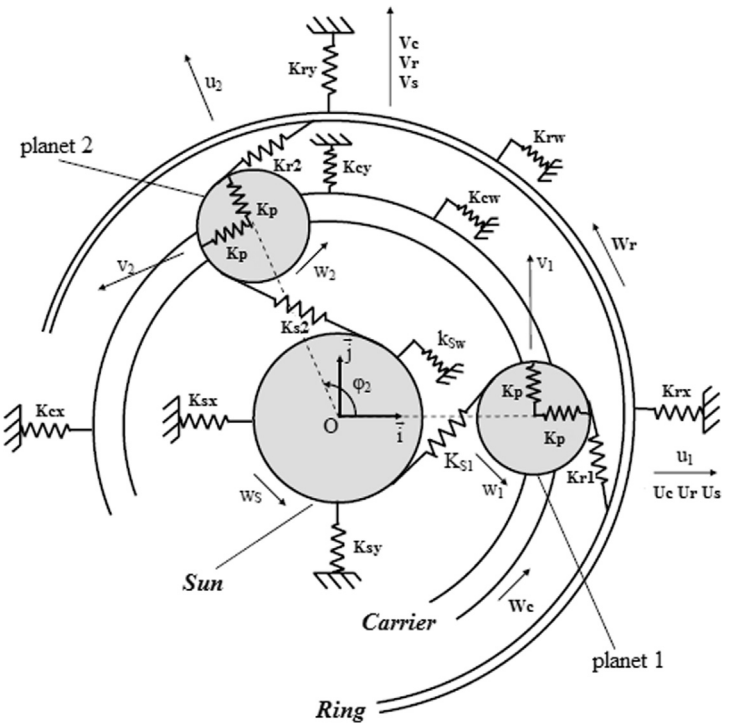

Fig. 1. Dynamic model of a planetary gear set.

2. Modeling of vibration signal

2.1. Dynamic model of a planetary gear set

In order to simulate the dynamic behavior of a planetary gearbox, a linear two-dimensional lumped parameter dynamic model [9] of a planetary gear set is adopted, as shown in Fig. 1. The sun, the carrier, the ring and the N planets are considered as stiff bodies. Bearings are modeled by a linear spring. Mesh interfaces between gear bodies are modeled by linear spring acting on the direction of the meshing force. Each component has three degrees of freedom: two translations along the x- and y-axes, respectively $(U_i,\ V_i)$ and one rotation around the pinion-axis (W_i) with $i \in$ (sun, ring, carrier, planet$_1$, .., planet$_N$). The local coordinate system is fixed on the carrier. As a consequence, all displacements are described with respect to the frame tied to the carrier, which is rotating with a constant speed ω_c. The damping will be introduced later as a proportional one. The equations of motion for this dynamic model can be found in [21].

2.2. Modeling of bearing stiffness and mesh stiffness function

Bearing stiffness have constant values as follows:

- K_{ix} and K_{iy} are the radial stiffness of each bearing component and are assumed equal on both x- and y-axes;
- K_{iw} is the torsional stiffness.

The mesh stiffness is time varying. It is approximated as a square wave form. Fig. 2 (a) and (b) display the variation of the mesh stiffness sun-planet$_1$, sun-planet$_2$, planet$_1$-ring, and planet$_2$-ring. The stiffness variation is due to the alternation between one and two pairs of teeth in contact.

An offset between mesh stiffness functions is observed due to the multiplicity of meshes on the same gear. It can be determined as follows [36]:

- angular offset 1: between sun and planet i $\gamma_{Si} = \dfrac{\varphi_i Z_S}{2\pi}$;
- angular offset 2: between planet i and ring $\gamma_{iR} = \dfrac{\varphi_i Z_R}{2\pi}$

Table 1 presents the geometric and physical parameters of the investigated planetary gearbox.

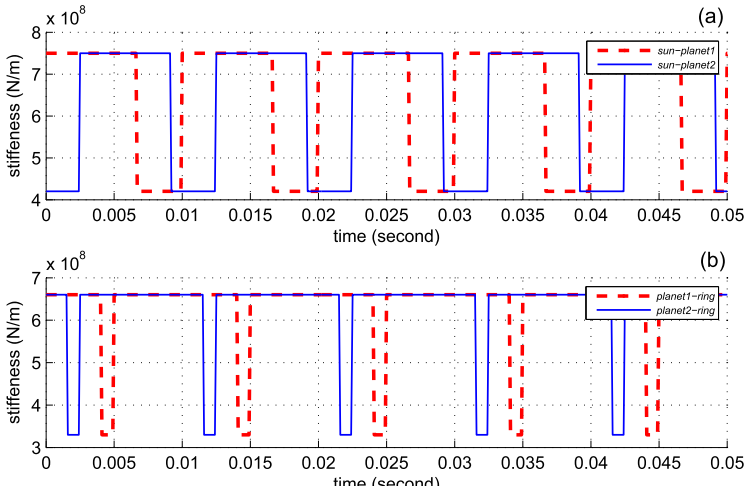

Fig. 2. Mesh stiffness function, (a) sun-planets, (b) planets-ring.

Table 1
Physical and geometric parameters of a planetary gear set [21].

Parameters	Sun gear	Planet gear	Ring gear	Carrier
Number	1	4	1	1
Number of teeth	39	27	93	–
Modulus	2	2	2	–
Pressure angle	20°	20°	20°	–
Mass (kg)	2.3	0.885	2.94	15
Base circle radius (m)	0.078	0.054	0.186	0.132
Bearing stiffness	$K_{sx} = K_{sy} = K_{px} = K_{py} = K_{rx} = K_{ry} = K_{cx} = K_{cy} = 10^8$			
	$K_{sw} = 0$	$K_{pw} = 0$	$K_{rw} = 10^{15}$	$K_{cw} = 0$
Input torque (Nm)	150	–	–	–
Input speed (rpm)	2183.6	–	–	–

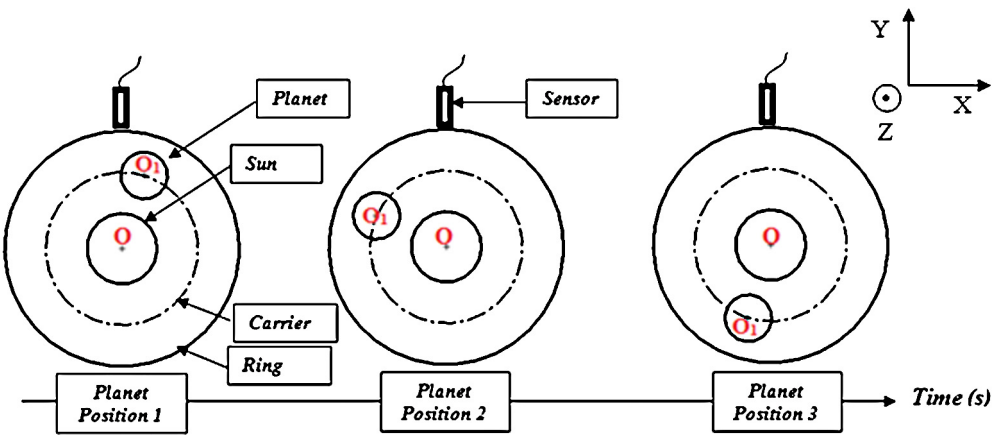

Fig. 3. Different positions occupied by the planet in one-carrier rotation.

3. Mathematical formulation of the modulation phenomenon

3.1. Improvement of Hanning function

As shown in Fig. 3, the planet can occupy different positions in one carrier period rotation because it revolves around (OZ) and (O_1Z). Since we investigate a planetary gear-set with fixed ring, the distance between each planet and the sensor location is time varying.

There is a succession of coming closer and going further of the planet from the location of the transducer, which causes a modulation in the resultant vibration acquired by the sensor. To model this phenomenon, an approach based on the

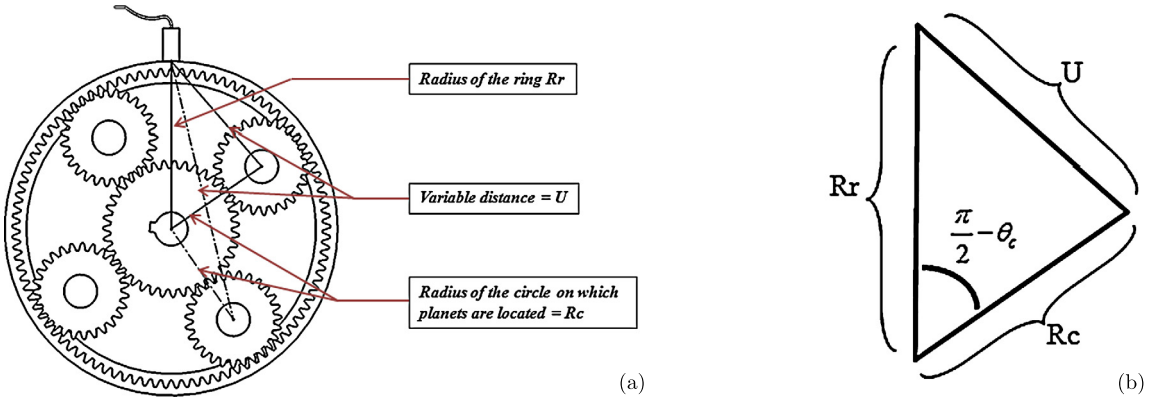

Fig. 4. Clarification of the time-varying distance U: (a) general view, (b) zoom in on the triangle (θ_c: instantaneous angular position of the carrier).

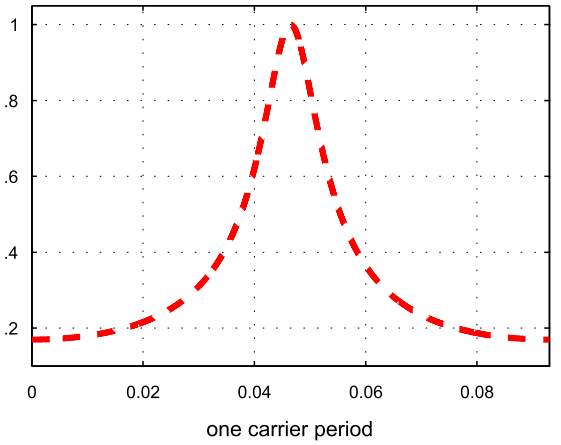

Fig. 5. Hanning function improved with physical characteristics.

geometric construction shown in Fig. 4 is adopted. It is noticed that the distance U separating the center of the planet and the position of the sensor is time varying depending on the angular position of the carrier θ_c.

By applying the law of cosines, the expression of the distance U is given by Eq. (1):

$$U = \sqrt{R_r^2 + R_c^2 - 2\,R_r\,R_c \sin(\theta_c)} \tag{1}$$

As seen in Fig. 4(b), the line U is linking two points: the first point is a fixed one at the location of the transducer and the other point is the rotating center of the planet. Hence, when the planet moves away from the location of the sensor, the distance U increases and the energy level of the vibration signal will decrease. Therefore, the modulation function MF is inversely proportional to U, and it can be written as:

$$MF = \frac{1}{U} = \frac{1}{\sqrt{R_r^2 + R_c^2 - 2\,R_r\,R_c \sin(\theta_c)}} \tag{2}$$

Fig. 5 presents a plot of MF for one carrier rotation period. As shown in Eq. (2), MF is derived only from the physical and geometric parameters of the planetary gearbox and could be an interesting tool to define the time-varying vibration transmission path. It was mentioned previously that vibration modulation was induced by the rotation of the carrier. So, the maximum of the MF curve corresponds to the closest position of the planet to the transducer and the minimum of the curve defines the farthest position. The function is not attenuated completely when the planet is in the farthest position because the sensor continues to acquire vibrations somehow.

In the literature, the Hanning or Hamming functions are usually used to consider variable vibration transmission paths. The example given in [2], presented in Fig. 6 (reproduced with kind permission of Elsevier) shows that the attenuation is controlled by modifying the values of α and β arbitrarily. But, in our case, only the physical and geometric parameters of the system are responsible for defining the optimal shape of the modulation function MF. For instance, by modifying the values of R_c and keeping the value of R_r constant as summarized in Table 2, the flatness of MF changes as shown in Fig. 7.

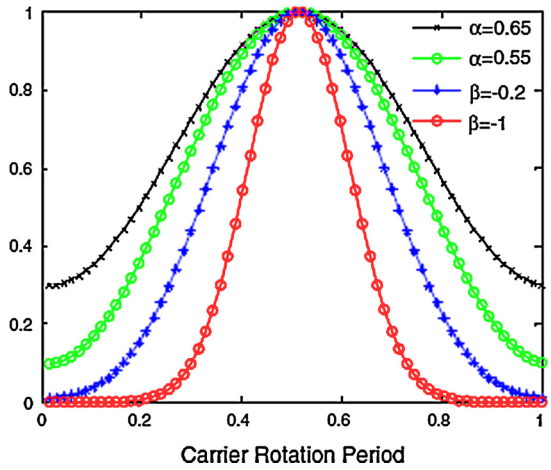

Fig. 6. Hanning function used in the literature [2].

Table 2
Different values of the radius of the carrier.

R_r			
R_c	$1.1 \times R_c$	$1.2 \times R_c$	$1.3 \times R_c$
Red	blue	magenta	black

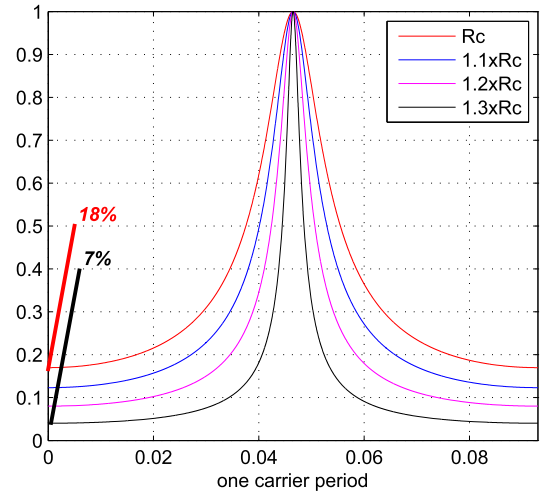

Fig. 7. Influence of the modification of the geometric characteristics on MF.

It is well noticed that when the value of R_c increases, the flatness of MF decreases. To explain this, it is necessary to remind the kinematic scheme of a planetary gearbox. Since R_r is kept constant, the radius of a planet has to decrease when the value of R_c increases. Therefore, as shown in Fig. 8, the bigger the value of R_c is, the smaller the dimension of the planet is.

In addition, the transducer lacks information when the planet is at the farthest position from the location of the transducer. One can observe in Fig. 7 that, for the red curve corresponding to the smallest value of R_c, the transducer is able acquire 18% of the vibration from the planet and, for the black one, the transducer can acquire only 7% of the vibration. Furthermore, as it will be later shown in Fig. 9, when MF becomes more and more flat (i.e. when the planet becomes bigger), the overlap between the MF s of two planets will be bigger due to the increase of the radius of the planet. Consequently, either the shape of the MF or the size of the overlap between two MF s of two consecutive planets are controlled and defined by the physical and geometric parameters of the planetary gearbox.

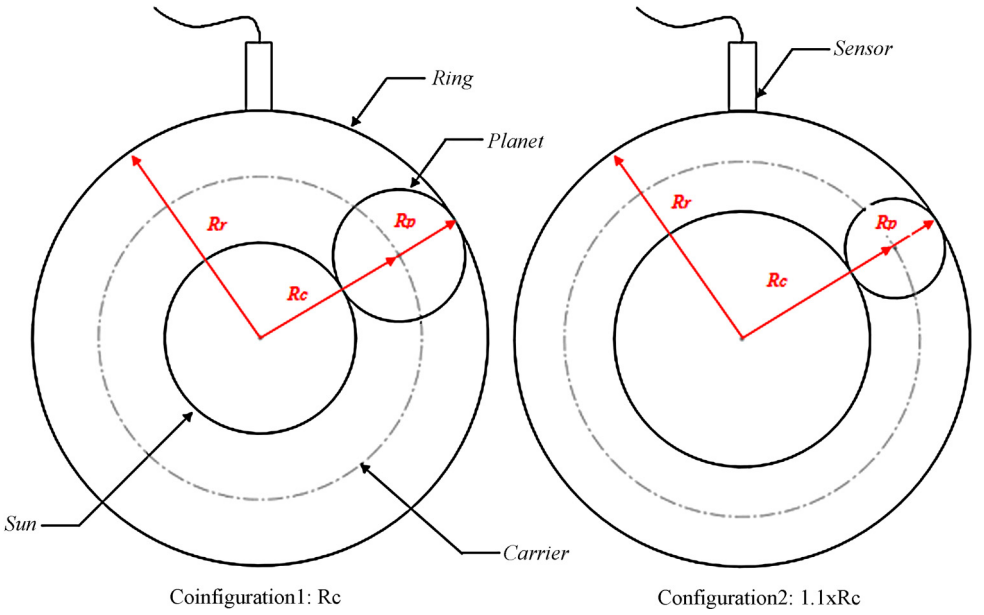

Fig. 8. Two configurations.

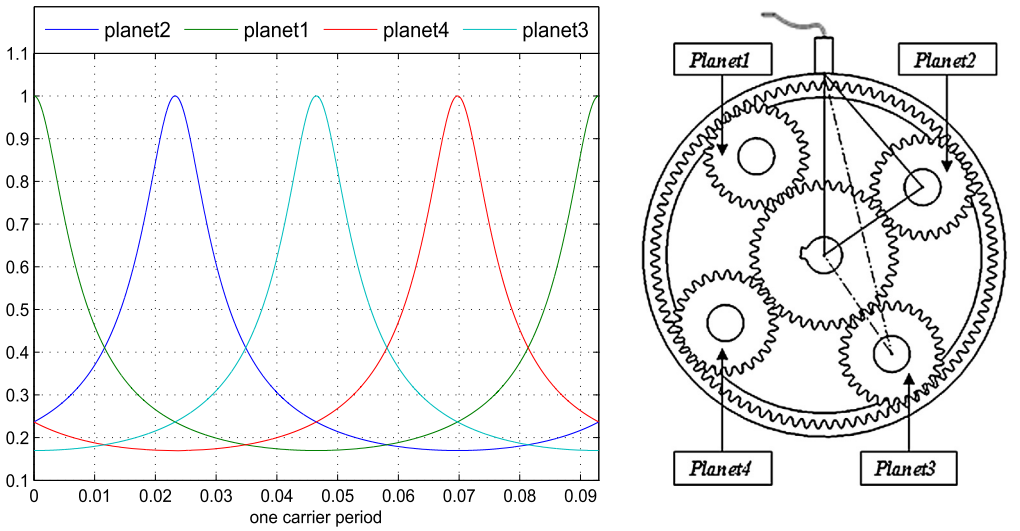

Fig. 9. MF for four planets.

3.2. Impact of each planet on the resultant vibration

The vibration signal collected by a sensor is influenced by the instantaneous position of each planet and by its number. Taking the example of four planets, four modulation functions, presented in Fig. 9, will influence the resultant vibration signal.

Since all displacements are described with respect to the rotating frame (section 2.1), the resultant vibration is not modulated by the rotational motion of the planets because the latter rotate with the frame. Fig. 10 presents the methodology allowing one to incorporate the vibration signal without modulation within the MF to obtain the impact of each planet alone on the resultant vibration.

The first row of Fig. 10 displays vibration components on the y-axis of the ring gear simulated with respect to the carrier, while the second row shows four modulation functions, since there are four planets. The last row presents the impact of each planet alone on the overall vibration components.

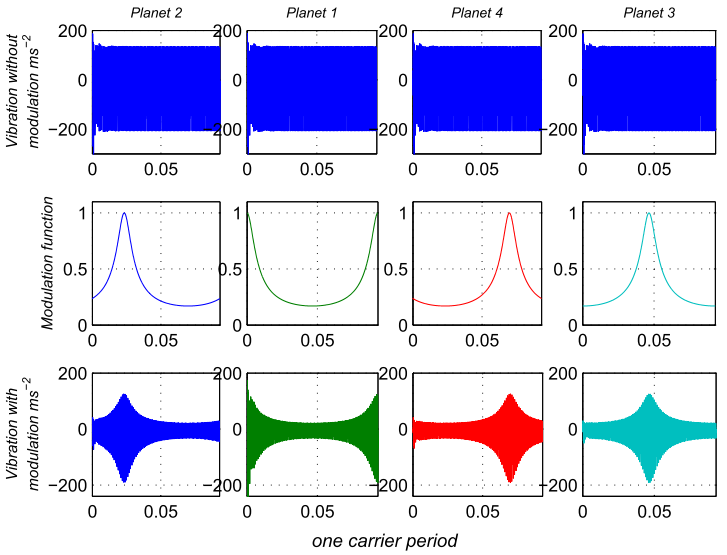

Fig. 10. Contribution of each planet alone to the modulated signal.

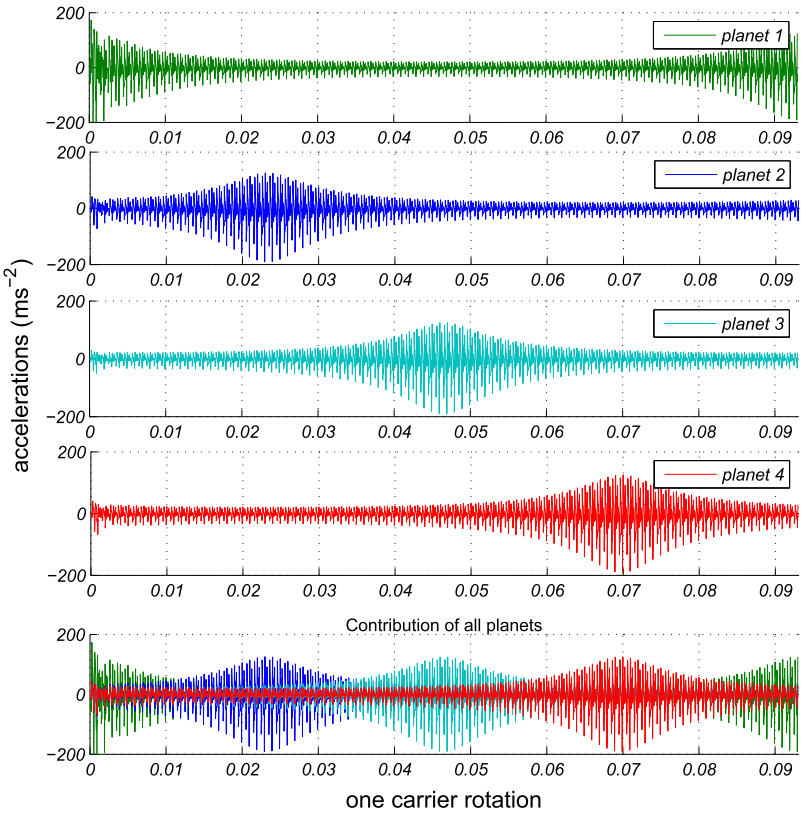

Fig. 11. Contribution of each planet to the modulation phenomenon.

4. Modeling of the overall vibration signal

As shown in section 3.2, the passage of each planet near the location of the sensor influences the vibration signal collected by the transducer. Each planet, alone, has an impact, as presented in Fig. 10. Fig. 11 explains how to localize each modulation in the right position in the overall vibration signal. The methodology is explained below.

The last sub-figure of Fig. 11 presents only a superposition without summation of the vibration induced by each planet alone to clarify the modulation phenomenon and to define the overlap between the vibration signal collected from each

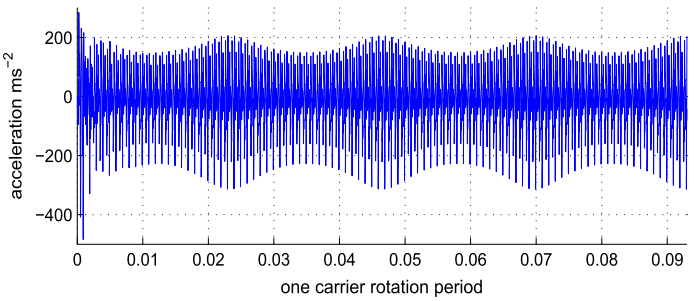

Fig. 12. Overall simulated vibration signal on the y-axis of the ring gear.

planet alone. But, in the real case, the sensor collects vibration signals from all planets at the same time. In other words, the signal acquired by the transducer is a summation of each vibration signal influenced by only one planet at each time presented in the four first sub-figures of Fig. 11. Fig. 12 shows the acceleration signal on the vertical axis of the fixed ring gear within one carrier period rotation for a healthy planetary gear-set according to the summation, which can be written as:

$$V = \sum_{i=1}^{N} \left(\frac{1}{\sqrt{R_r^2 + R_c^2 - 2\,R_r\,R_c \sin(2\pi f_c t + i\frac{2\pi}{N})}} \cdot V_i \right) \tag{3}$$

where R_r, R_c, f_c and N are respectively the radius of the ring, the radius of the carrier, the frequency of the carrier, and the number of planets. V_i is the vibration component described with respect to the carrier's frame.

5. Scheme of the numerical simulation

Fig. 13 presents the scheme of the numerical simulation, including all information about algorithms, step, increment time...

6. Resultant vibration analysis

As seen in Fig. 12, four modulations are clearly observed in one carrier period rotation induced by the passage of the four planets close to the location of the sensor. The amplitude of the overall vibration signal is greater than the amplitude of the vibration signal induced by each planet alone, since the sensor will acquire the vibrations from all planets in the same time, and each planet will contribute to the overall vibration depending on its position with respect to the sensor's location.

Fig. 14 displays the spectrum of the vibration signal with a sampling frequency $f_s = 50$ kHz. The gear-mesh frequency, $GMF = 1000$ Hz, is well identified with its harmonics.

A zoom section between 1800 Hz and 3500 Hz is displayed in Fig. 15, with a logarithmic scale to highlight the presence of the modulation phenomenon.

Based on Table 1 and the formulas presented below, the rotation frequency of the carrier is obtained:

$$f_s = \frac{N_s}{60} = 36.39\,\text{Hz}: \text{ sun frequency; } r = \frac{Z_s}{Z_s + Z_r} = 0.2955: \text{ ratio (planetary);}$$

$f_c = r \times f_s = 10.75\,\text{Hz}:$ carrier frequency.

In Fig. 15, two gear-mesh frequency harmonics $H1_{GMF} = 2000$ Hz and $H2_{GMF} = 3000$ Hz are displayed and some side-bands are observed on both sides of the components. Table 3 presents the main sidebands observed around these two harmonics.

The obtained results are in accordance with those presented in [23], issued from experimental tests and shown in Fig. 16 (a) for healthy cases (reproduced with kind permission of Elsevier). Frequency bands from each side (green color) of the gear mesh frequency range at $f_m \pm 3f_c$, $f_m \pm 6f_c$, ..., $f_m \pm iN \times f_c$ $\forall\, i \in \mathbb{N}^*$, with N the number of planets, are clearly evidenced. In our case, the same behavior is observed: the frequency bands are located from each side at $f_m \pm iN \times f_c$ $\forall\, i \in \mathbb{N}^*$, as shown in Fig. 15.

7. Conclusions

In this paper, an improved Hanning function is proposed to take into account the variable vibration transmission path in planetary gears. A dynamic model is used to build all vibration sources including sun, planets, and ring gear. A modulation function is proposed as a time-varying distance between the position of the planets and the location of the transducer.

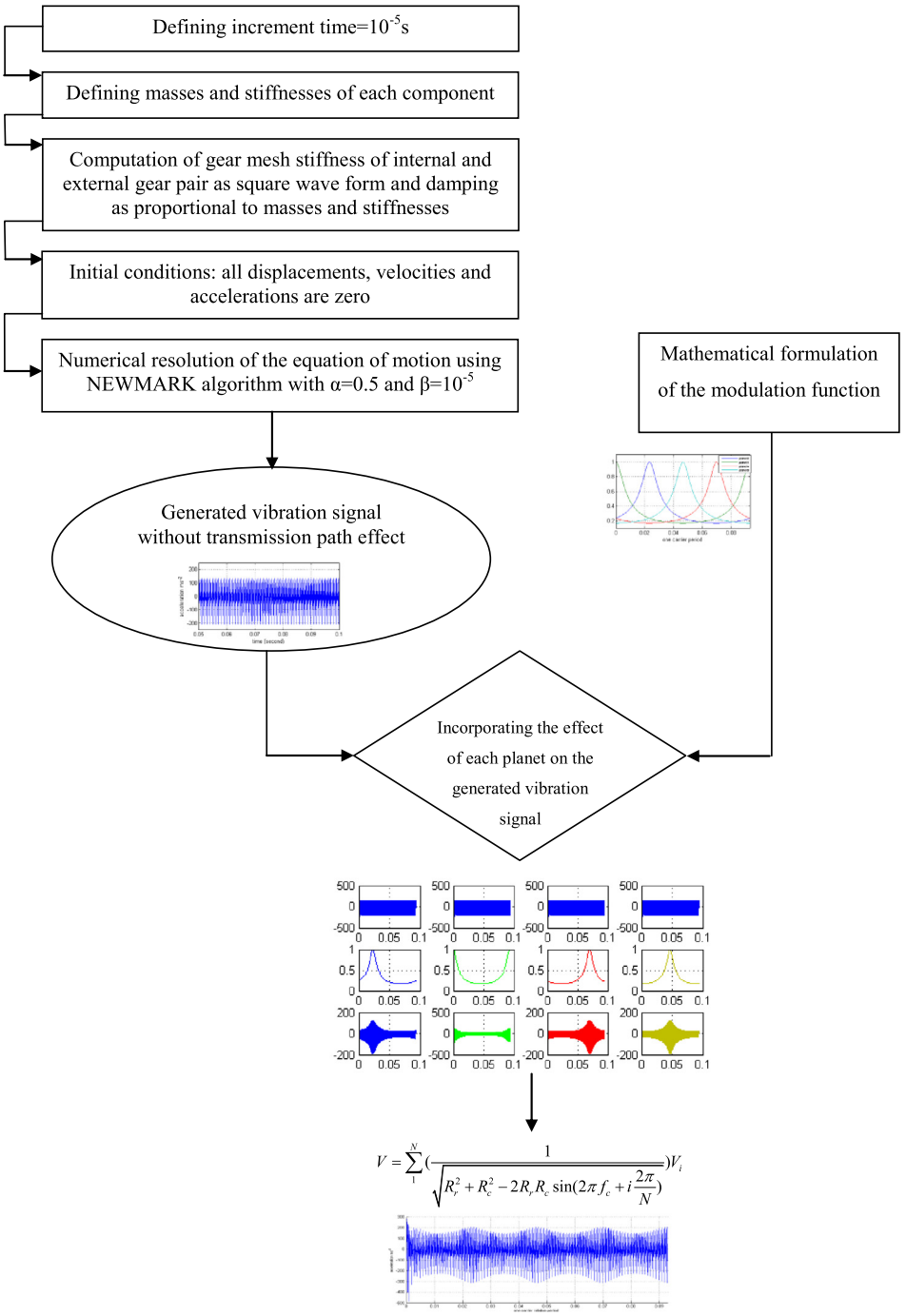

Fig. 13. Scheme of the numerical simulation.

Compared to other works in the literature, the proposed window function is controlled by the geometric and physical parameters of the planetary gearbox. Moreover, given the latter, the attenuation of the modulation function is estimated; it defines how much vibration can be captured by the transducer when the planet is in the farthest position from the sensor location. Vibration properties are validated with the experimental results reported in [23]. Finally, when adopting the methodology consisting in combining the lumped parameter model with the amplitude modulation by window function, one would be well advised to use the proposed window function, since it describes with more reality the mechanisms leading to the modulation phenomenon.

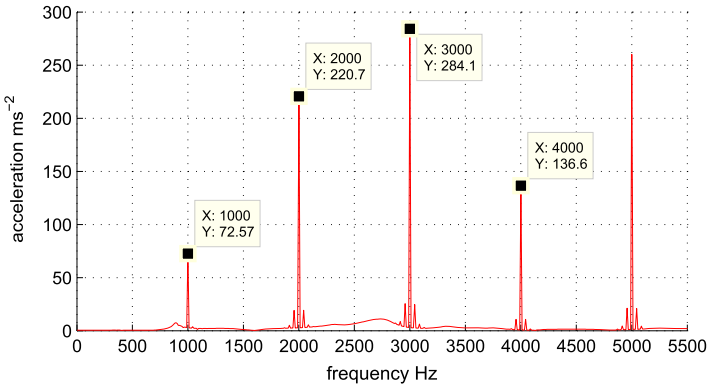

Fig. 14. Spectrum of the acceleration measured on the ring gear on the y-axis.

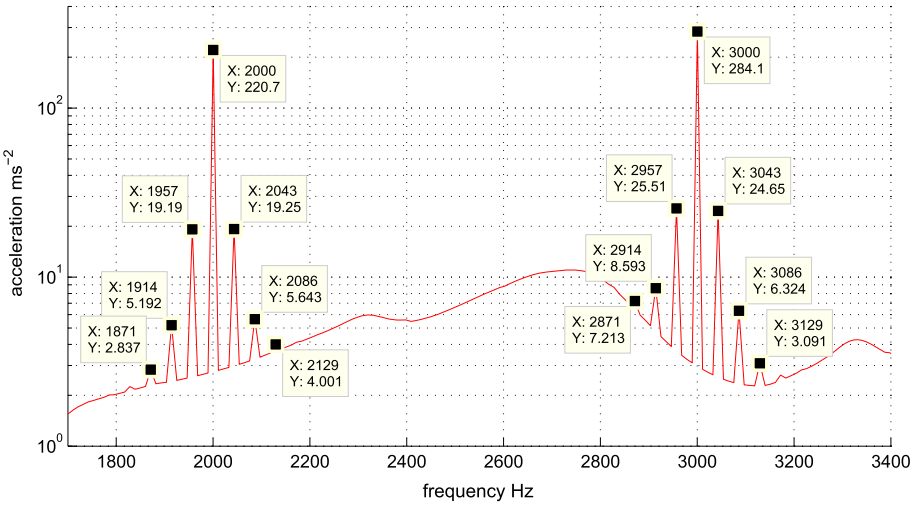

Fig. 15. Zoom-in on the range 1800 Hz–3500 Hz.

Table 3
Values of the frequencies and their correspondence.

Frequencies (Hz)	Correspondence
2000	$H1_{GMF}$
2043–1957	$H1_{GMF} \pm 4 \times f_c$
2086–1914	$H1_{GMF} \pm 8 \times f_c$
2129–1871	$H1_{GMF} \pm 12 \times f_c$
3000	$H2_{GMF}$
3043–2957	$H2_{GMF} \pm 4 \times f_c$
3086–2914	$H2_{GMF} \pm 8 \times f_c$
3129–2871	$H2_{GMF} \pm 12 \times f_c$

Acknowledgements

This work was partially supported by the National School of Engineers of Sfax (ENIS)/Laboratory of Mechanics, Modelling and Production (LA2MP) and the National Centre of Research and Development (NCRD) in Poland under research project No. PBS3/B6/21/2015.

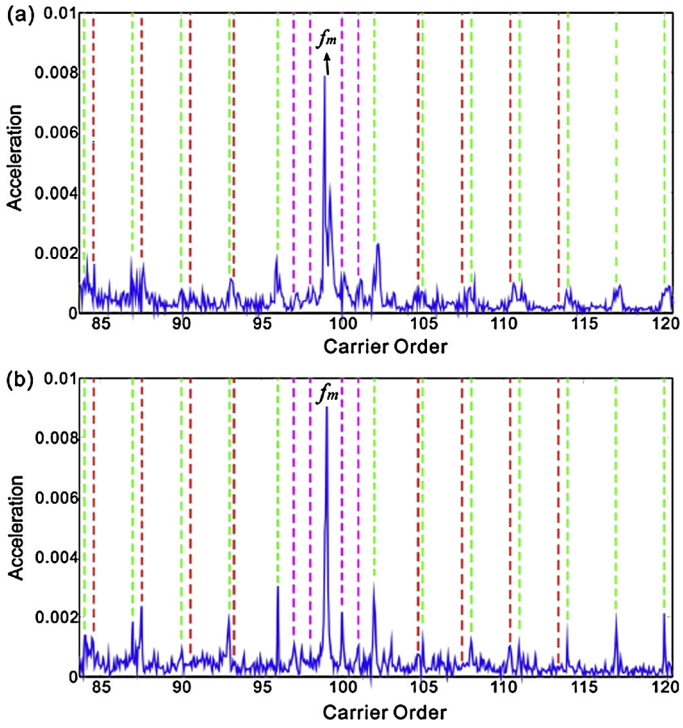

Fig. 16. (a) Original measured vibration spectrum around the fundamental gear-mesh frequency of the planetary gear set, and (b) vibration spectrum after the proposed algorithm around the fundamental gear-mesh frequency of the planetary gear set [23].

References

[1] X. Liang, M.J. Zuo, M.R. Hoseini, Vibration signal modeling of a planetary gear set for tooth crack detection, Eng. Fail. Anal. 48 (2015) 185–200.
[2] L. Liu, X. Liang, M.J. Zuo, Vibration signal modeling of a planetary gear set with transmission path effect analysis, Measurement 85 (2016) 20–31.
[3] N. Feki, M. Karray, M.T. Khabou, F. Chaari, M. Haddar, Frequency analysis of a two-stage planetary gearbox using two different methodologies, C. R. Mecanique 345 (2017) 832–843.
[4] L. Zhang, Y. Wang, K. Wu, R. Sheng, Q. Huang, Dynamic modeling and vibration characteristics of a two-stage closed-form planetary gear train, Mech. Mach. Theory 97 (2016) 12–28.
[5] M. Inalpolat, A. Kahraman, A theoretical and experimental investigation of modulation sidebands of planetary gear sets, J. Sound Vib. 323 (2009) 677–696.
[6] M. Inalpolat, A. Kahraman, A dynamic model to predict modulation sidebands of a planetary gear set having manufacturing errors, J. Sound Vib. 329 (2010) 371–393.
[7] Z. Feng, M.J. Zuo, Vibration signal models for fault diagnosis of planetary gearboxes, J. Sound Vib. 331 (2012) 4919–4939.
[8] T.R. Pattabiraman, K. Srinivasan, K. Malarmohan, Assessment of sideband energy ratio technique in detection of wind turbine gear defects, Case Stud. Mech. Syst. Signal Process. 2 (2015) 1–11.
[9] W. Bartelmus, F. Chaari, R. Zimroz, M. Haddar, Modelling of gearbox dynamics under time-varying nonstationary load for distributed fault detection and diagnosis, Eur. J. Mech. A, Solids 29 (2010) 637–646.
[10] P. Sondkar, A. Kahraman, A dynamic model of a double-helical planetary gear set, Mech. Mach. Theory 70 (2013) 157–174.
[11] L. Zhang, Y. Wang, K. Wu, R. Sheng, Three-dimensional modeling and structured vibration modes of two-stage helical planetary gears used in cranes, Hindawi: Shock Vib. 2017 (2017) 9864959.
[12] Y. Guo, R.G. Parker, Dynamic modeling and analysis of a spur planetary gear involving tooth wedging and bearing clearance nonlinearity, Eur. J. Mech. A, Solids 29 (2010) 1022–1033.
[13] V.K. Ambarisha, R.G. Parker, Nonlinear dynamics of planetary gears using analytical and finite element models, J. Sound Vib. 302 (2007) 577595.
[14] M.B. Sanchez, M. Pleguezuelos, J.I. Pedrero, Approximate equations for the meshing stiffness and the load sharing ratio of spur gears including hertzian effects, Mech. Mach. Theory 109 (2017) 231–249.
[15] Z. Chen, Y. Shao, Mesh stiffness calculation of a spur gear pair with tooth profile modification and tooth root crack, Mech. Mach. Theory 62 (2013) 63–74.
[16] X. Liang, H. Zhang, L. Liu, M.J. Zuo, The influence of tooth pitting on the mesh stiffness of a pair of external spur gears, Mech. Mach. Theory 106 (2016) 1–15.
[17] A. Saxena, A. Parey, M. Chouksey, Time varying mesh stiffness calculation of spur gear pair considering sliding friction and spalling defects, Eng. Fail. Anal. 70 (2016) 200–211.
[18] H. Ma, Z. Li, M. Feng, R. Feng, B. Wen, Time-varying mesh stiffness calculation of spur gears with spalling defect, Eng. Fail. Anal. 66 (2016) 166–176.
[19] F. Chaari, W. Baccar, M. Slim Abbes, M. Haddar, Effect of spalling or tooth breakage on gearmesh stiffness and dynamic response of a one-stage spur gear transmission, Eur. J. Mech. A, Solids 27 (2008) 691–705.
[20] A. Kahraman, Natural modes of planetary gear trains, J. Sound Vib. 173 (1) (1994) 125–130.
[21] F. Chaari, Contribution à l'étude du comportement dynamique des trains épicycloïdaux à denture droite en présence de défauts, PhD thesis, ENI, Sfax, Tunisia, 2005.
[22] F. Chaari, T. Fakhfakh, M. Haddar, Analytical modelling of spur gear tooth crack and influence on gearmesh stiffness, Eur. J. Mech. A, Solids 28 (2009) 461–468.

[23] L. Hong, Y. Qu, J. Singh Dhupia, S. Sheng, Y. Tan, Z. Zhou, A novel vibration-based fault diagnostic algorithm for gearboxes under speed fluctuations without rotational speed measurement, Mech. Syst. Signal Process. 94 (2017) 14–32.
[24] J. Lin, R.G. Parker, Mesh stiffness variation instabilities in two-stage gear systems, J. Vib. Acoust. 124 (2002) 68–76.
[25] J. Meagher, X. Wu, D. Kong, C.H. Lee, A comparison of gear mesh stiffness modeling strategies, in: Conference Proceedings of the Society for Experimental Mechanics, vol. 12, Jacksonville, FL, USA, 1–4 February 2010, 2010, pp. 255–263.
[26] S. Jia, I.M. Howard, Comparison of localised spalling and crack damage from dynamic modelling of spur gear vibrations, Mech. Syst. Signal Process. 20 (2) (2006) 332–349.
[27] J. Zhan, M. Fard, R. Jazar, A CAD-FEM-QSA integration technique for determining the time-varying meshing stiffness of gear pairs, Measurement 100 (2017) 139–149.
[28] R.G. Parker, S.M. Vijayakar, T. Imajo, Non-linear dynamic response of a spur gear pair: modelling and experimental comparisons, J. Sound Vib. 237 (3) (2000) 435–455.
[29] P. Marques, R. Martins, J. Seabra, Analytical load sharing and mesh stiffness model for spur/helical and internal/external gears towards constant mesh stiffness gear design, Mech. Mach. Theory 113 (2017) 126–140.
[30] A. Mbarek, A. Hammamia, A. Fernandez Del Rincon, F. Chaari, F. Viadero Rueda, M. Haddar, Effect of load and meshing stiffness variation on modal properties of planetary gear, Appl. Acoust. (2017), in press, https://doi.org/10.1016/j.apacoust.2017.08.010.
[31] F. Viadero, A. Fernandez, M. Iglesias, A. de-Juan, E. Liano, M.A. Serna, Non-stationary dynamic analysis of a wind turbine power drivetrain: offshore considerations, Appl. Acoust. 77 (2014) 204211.
[32] A. Fernandez, M. Iglesias, A. de-Juan, P. Garcia, R. Sancibrian, F. Viadero, Gear transmission dynamic: effects of tooth profile deviations and support flexibility, Appl. Acoust. 77 (2014) 138149.
[33] A. Fernandez-del-Rincon, M. Iglesias, A. de-Juan, A. Diez-Ibarbia, P. Garcia, F. Viadero, Gear transmission dynamics: effects of index and run out errors, Appl. Acoust. (2015), in press, https://doi.org/10.1016/j.apacoust.2015.11.012.
[34] V. Abousleiman, P. Velex, A hybrid 3D finite element/lumped parameter model for quasi-static and dynamic analyses of planetary/epicyclic gear sets, Mech. Mach. Theory 41 (2006) 725748.
[35] C.G. Cooley, C. Liu, X. Dai, R.G. Parker, Gear tooth mesh stiffness: a comparison of calculation approaches, Mech. Mach. Theory 105 (2016) 540553.
[36] R.G. Parker, J. Lin, Modelling, Modal Properties, and Mesh Stiffness Variation Instabilities of Planetary Gears, NASA/CR–2001-210939, ARL-CR-462, NASA, 2001.